

Improved Start-Up Scenario for Single-Stage Electronic Ballast

Tsai-Fu Wu, *Senior Member, IEEE*, and Yong-Jing Wu, *Student Member, IEEE*

Abstract—This paper presents improved start-up scenario for single-stage electronic ballast derived with synchronous switch technique (SST). Based on the SST, the derivation of a single-stage inverter (SSI) used for realizing the ballast is then addressed. The SSI can achieve both high power factor and ballasting function. During lamp start-up transition, power imbalance may exist between the power factor correction semi-stage and the ballast semi-stage, and filament preheating is an important issue. Power imbalance usually results in a high dc-link voltage which, in turn, imposes high stress on the switching devices. Investigation of the ballast operation is conducted, from which control strategies for reducing component stresses and hot resistance detection circuits for minimizing electrode sputtering are therefore proposed. Hardware measurements have verified that on-off tests are higher than 18 000 times without significant sputtering.

Index Terms—Single-stage electronic ballast.

I. INTRODUCTION

ELECTRONIC ballasts for gaseous discharge lamps received great attention in recent years due to their merits of light weight, small size and high efficacy. Most of the electronic ballasts are realized with resonant inverters operating at high frequency. The ballasts driven by the voltage source obtained from rectifying and smoothing the ac mains essentially induce harmonic current distortion and lower power factor. To solve these problems, a power factor corrector is usually cascaded in front of a ballast. This solution, however, results in a complicated system configuration, high cost and large size.

Electronic ballast applications with single-stage inverters have been widely discussed in the literature [1]–[20], improving the drawbacks mentioned above. Most of them were dedicated in studying the steady state operation of ballast systems, while did they seldom discuss the behavior of ballasts during lamp preheating stage. If there exists power imbalance, the dc-link voltage in the single-stage ballast may increase beyond the steady state voltage significantly, especially at light load operation. Thus, devices with high voltage ratings have to be used, increasing cost significantly. In [20], the ballast maintains constant dc-link voltage by controlling the switching frequency. This control method results in complicating circuit design, increasing cost and deteriorating in reliability. In addition,

since the switching frequency is varying, the output power of the lamp cannot be kept constant.

This paper presents the analysis, design and practical consideration of a single-stage electronic ballast with only open-loop control on the dc-link voltage at start-up stage, reducing component stresses and simplifying circuit design significantly. The power stage of the proposed ballast with high power factor is the combination of a buck-boost converter and a half-bridge series-resonant parallel-loaded inverter (SRPLI). The ballast can be derived with the synchronous switch technique (SST) [21]. Transient and steady state behaviors of the ballast system are investigated, on which the voltage and current stresses imposed on components are examined. Circuits for minimizing the component stresses are therefore proposed.

Filaments need to be properly preheated to prevent electrodes from sputtering. In the paper, a circuit used for detecting if the filaments are properly preheated is presented. Experimental results are provided to verify the theoretical analysis.

II. ANALYSIS OF THE PROPOSED SINGLE-STAGE INVERTER

Fig. 1(a) shows the schematic diagram of a buck-boost converter and an SRPLI in cascade connection. The buck-boost converter achieves power factor correction and the SRPLI realizes lamp driving feature. Properly relocating switch M_3 , as shown in Fig. 1(b), can establish a drain-drain (D-D) common node for M_2 and M_3 . Thus, the SST presented in [21] can be used to integrate these two stages through a replacement of M_2 and M_3 with an inverted T -type synchronous switch M_{ss} , which results in the SSI depicted in Fig. 1(c). This SSI can fulfill the same functions as and possess similar characteristics to the individual stages shown in Fig. 1(a). Unlike conventional analysis in which the inverter is sequentially described according to its operation modes, analysis of the SSI is conducted with its two semi-stages, namely buck-boost semi-stage and ballast semi-stage, separately and then, the analytical results are combined together. This analytical procedure can explore more physical insights into the SSI.

When switch M_{ss} is operated with a fixed frequency and a constant on time over at least half a line period, the envelope of the input current i_{in} will sinusoidally follow the line voltage and present a power factor close to unity. The peak value of i_{in} within half a line period can be expressed as follows:

$$i_{in(\text{peak})}(t) = \frac{V_I \sin(\omega t)}{L_{\text{pf}}} \cdot \frac{d}{f_s}, \quad 0 \leq t \leq \frac{T_I}{2} \quad (1)$$

Manuscript received July 6, 1999; revised December 3, 1999. Recommended by Associate Editor, L. R. Nerone. This work was supported by the National Science Council, Taiwan, R.O.C., under Project NSC 88–22B-E-194–031.

The authors are with Power Electronics Applied Research Laboratory (PEARL), Department of Electrical Engineering, National Chung Cheng University, Chia-Yi 621, Taiwan, R.O.C. (e-mail: tfwu@ee.ccu.edu.tw).

Publisher Item Identifier S 0885-8993(00)03376-7.

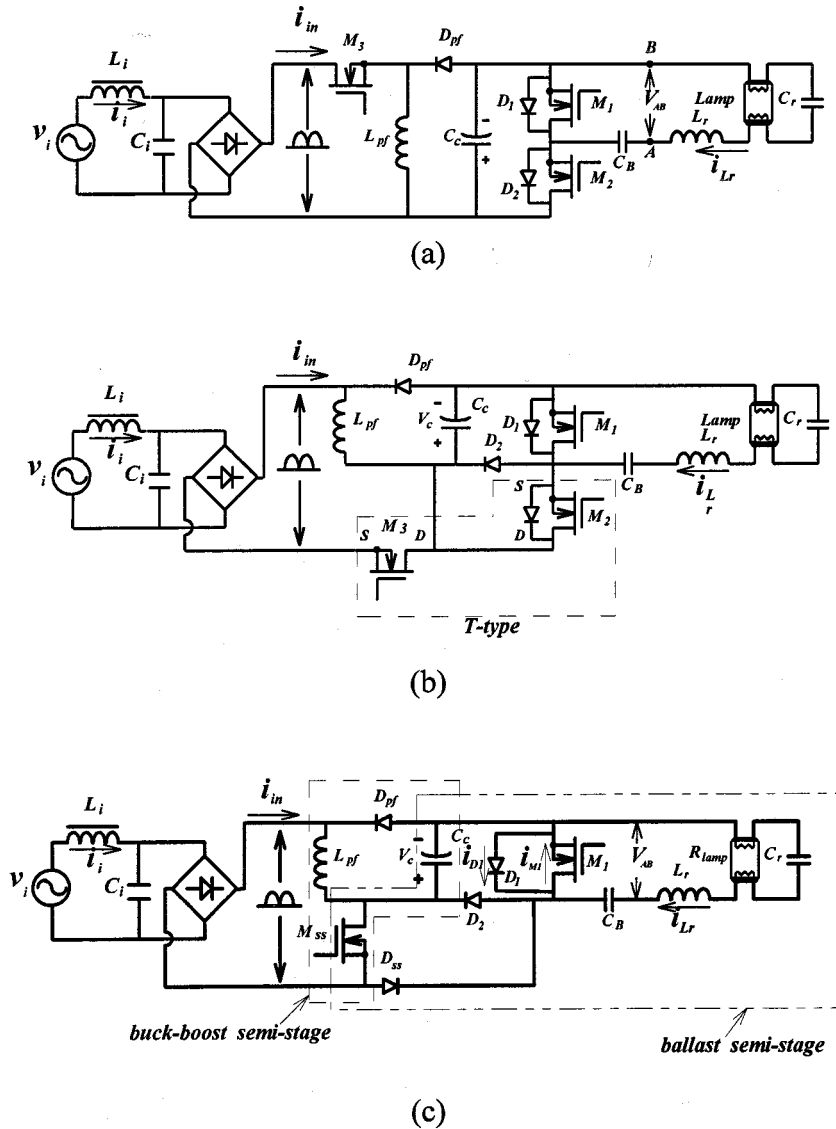


Fig. 1. Illustration of the discussed SSI derived from the buck-boost converter and the half-bridge SRPLI.

where V_I is the amplitude of line voltage, d is the duty ratio, ω_l is the line frequency and f_s is the switching frequency. The power (P_i) delivered to the buck-boost semi-stage can be calculated as

$$P_i = \frac{V_I^2 d^2 \int_0^{T_l} \sin^2(\omega_l t) dt}{T_l 2L_{pf} f_s} = \frac{V_I^2 d^2}{4L_{pf} f_s} \quad (2)$$

Equation (2) reveals that when L_{pf} and V_I are fixed, input power P_i varies with switching frequency f_s and duty ratio d . If input power P_i is equal to the power absorbed by the ballast semi-stage, the voltage V_c can be kept constant. On the other hand, if P_i is greater than the power absorbed by the ballast semi-stage, dc-link voltage V_c will increase indefinitely.

For the ballast semi-stage shown in Fig. 1(c), when switches M_1 , D_1 , M_{ss} and D_2 take turn on conducting, a square-wave

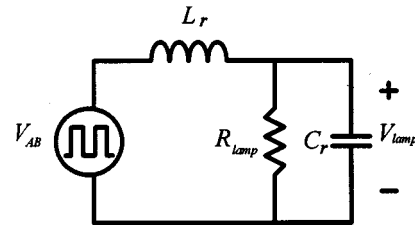


Fig. 2. An equivalent circuit of the half-bridge SRPLI, where the amplitude of V_{AB} is $V_c/2$.

voltage is generated to drive the lamp through an LC filter network. Assuming the blocking capacitance C_B is much larger than the resonant capacitance C_r , an equivalent circuit of the ballast semi-stage which is good for steady state analysis can be obtained and shown in Fig. 2, where the amplitude of V_{AB} is $V_c/2$. If the quality factor Q of the circuit is high enough, a fundamental frequency approximation method can be used to

analyze the circuit with high accuracy. With a fundamental frequency approximation method, lamp voltage V_{lamp} can be determined from the following equations:

$$V_{\text{lamp}} = \frac{V_s}{\sqrt{\left(1 - \left(\frac{f_s}{f_o}\right)^2\right)^2 + \left(\frac{f_s}{Qf_o}\right)^2}} \quad (3)$$

where

$$f_o = \frac{1}{2\pi\sqrt{L_r C_r}} \quad (4)$$

$$Q = \frac{R_{\text{lamp}}}{\sqrt{\frac{L_r}{C_r}}} \quad (5)$$

and V_s denotes the rms value of the fundamental component of square-wave voltage V_{AB} represented in a Fourier series. Using (3), (4) and (5), design of the ballast semi-stage can be completed with the determination of L_r , C_r and f_s . To properly operate the lamp, the determination of these values needs to take into account the following two operating conditions.

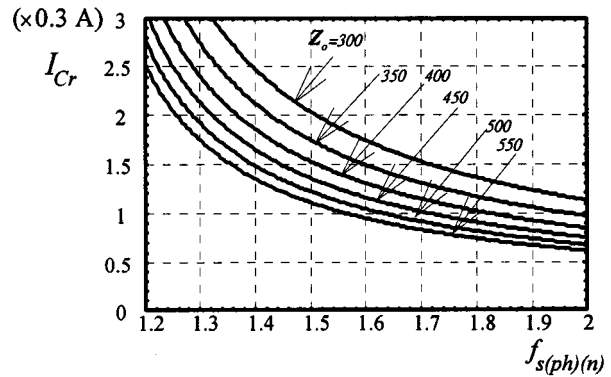
- 1) Before ignition, the output voltage V_{lamp} must be high enough to ignite the lamp.
- 2) After ignition, the lamp has to operate with a full power level.

These are basic requirements of a practical electronic ballast. Based on these considerations, switching frequency f_s is chosen to be close to the natural frequency f_o . With this frequency, it can be shown $|V_{\text{lamp}}| \approx Q|V_s|$ that from (3). The lamp can be ignited because Q is relatively high before ignition, and can be operated at the full power after ignition, at which Q drops to a smaller value. However, since the natural frequency f_o is higher than the resonant frequency $f_r (=f_o\sqrt{1-1/Q^2})$, large reactive current will be induced and flows through the switches. This would result in high current stress. To solve the problem, switching frequency f_s is set to near natural frequency f_o at startup transition. Then, switching frequency f_s is shifted to be close to resonant frequency f_r after the lamp is successfully ignited. Thus, the lamp is operated at full power and the current stress of the switches can be reduced.

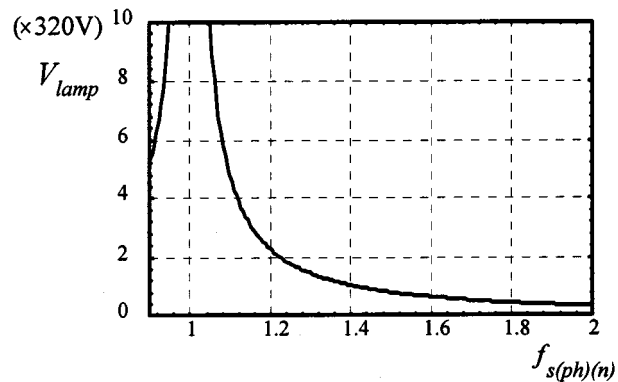
In practice, switching frequency $f_{s(\text{fl})}$ at full load is chosen to be slightly higher than resonant frequency f_r ; thus, the switches can always operate above the resonance to achieve a zero voltage switching (ZVS) at turn-on transition. To ensure a ZVS, switching frequency $f_{s(\text{fl})}$ must satisfy the following inequality:

$$f_o > f_{s(\text{fl})} \geq f_r = f_o\sqrt{1 - \frac{1}{Q^2}}. \quad (6)$$

According to the selected $f_s = f_{s(\text{fl})}$, a specified natural frequency f_o and a desired operating voltage V_{lamp} , the quality factor Q with respect to the full power level can be determined from (3). Inductance L_r and capacitance C_r can be therefore calculated from (4) and (5). These values can be uniquely determined for the full power operation of a given lamp.



(a)



(b)

Fig. 3. (a) The plots of preheating filament current I_{C_r} versus normalized switching frequency $f_{s(\text{ph})(n)}$ with Z_0 as a parameter. (b) The plots of lamp voltage V_{lamp} (before ignition) versus normalized switching frequency $f_{s(\text{ph})(n)}$.

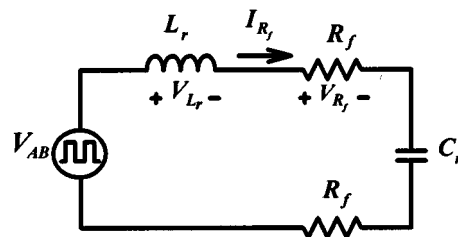


Fig. 4. An equivalent circuit of the ballast semi-stage in preheating duration.

III. PRACTICAL CONSIDERATIONS AND LIMITATIONS

A. Preheating of the Lamp Filaments

Operating an electronic ballast needs to take care not only the steady state operation but the preheating. Properly preheating the filaments becomes critically necessary to avoid deterioration of lamp life. Igniting a lamp at a low filament temperature requires a relatively high ignition voltage, causing bombardment and resulting in extremely sputtering on filaments. On the other hand, overheating the filaments will cause their coating material over evaporating and thermal shock. Both of the two improper preheating conditions engender sputtering and shortening their life. Lamp filaments must reach their emission temperature at

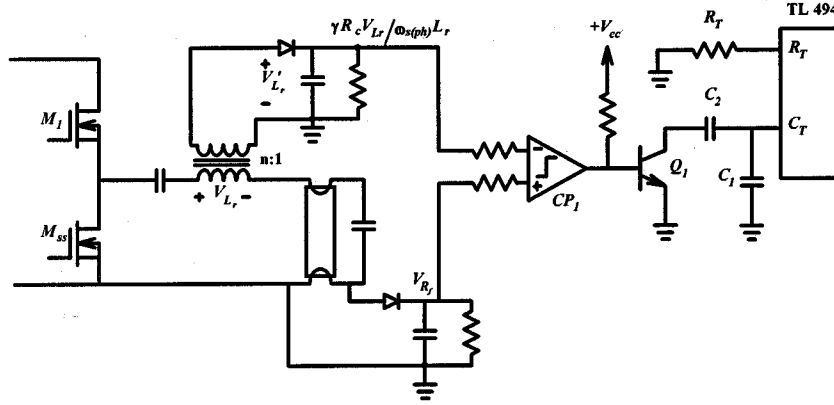


Fig. 5. Circuit for detecting preheating ratio $\gamma = R_h/R_c$.

starting stage to minimize electrode sputtering. The preheating ratio $\gamma (=R_h/R_c)$ of the hot resistance (R_h) of the electrodes to their cold resistance (R_c) is a proper index in knowing an approximate emission temperature, and the electrodes with such a ratio means that it reaches a temperature high enough for thermionic emission [22], [23].

Preheating time and current are two important factors in determining if electrodes reach a proper preheating ratio γ at the moment of igniting a lamp [23], [24]. The plots of filament current I_{C_r} and V_{lamp} versus $f_{s(\text{ph})(n)} (=f_{s(\text{ph})}/f_o)$, as shown in Fig. 3, provide the information for determining a proper preheating switching frequency $f_{s(\text{ph})}$, assuming the resistance R_{lamp} is infinite at this stage. According to the determined $Z_o (= \sqrt{L_r/C_r})$, preheating frequency $f_{s(\text{ph})}$ can be selected from the plots so as filament current I_{C_r} is high enough while the lamp voltage is not too high to generate significant glow current. In general, preheating time will increase to achieve a proper electrode temperature when the ballast operates at a higher preheating frequency $f_{s(\text{ph})}$. On the other hand, a lower preheating frequency $f_{s(\text{ph})}$ will shrink preheating time, while it may result in high lamp voltage, generating glow current and causing bombardment. Choosing a proper preheating frequency $f_{s(\text{ph})}$ can help filaments to reach a desired preheating ratio γ at ignition moment.

B. Detecting Preheating Ratio $\gamma = R_h/R_c$

Filament reaching its operating temperature at ignition moment can minimize sputtering. It is, however, difficult and inconvenient to directly sense the temperature to determine a proper moment for ignition. In literature [22], [23], researchers have proposed an indirect method to sense the temperature, which is to measure preheating ratio $\gamma = R_h/R_c$. Based on experiments, when $\gamma = 4-5$, it means the filaments have reached their thermionic emission temperature. With this information, engineers can design a proper preheating circuits for given lamps. In the following, analysis and design of a circuit for determining a proper γ is discussed.

To determine $\gamma = R_h/R_c$, one has to know R_h and R_c . For a given lamp, cool filament resistance R_c can be readily measured offline, while its hot resistance R_h has to measure online, complicating the determination of γ significantly. According to

the circuit shown in Fig. 4, we can obtain $R_h (=R_f)$ from V_{R_f} and I_{R_f} , and it is given as follows:

$$R_h = \frac{V_{R_f}}{I_{R_f}}. \quad (7)$$

In practice, sensing voltage is much easier than sensing current. In the design, V_{R_f} is measured directly from the voltage across the filament, while I_{R_f} is measured by way of inductor voltage V_{L_r} for the convenience of implementation. This is given as follows:

$$I_{R_f} = \frac{V_{L_r}}{\omega_{s(\text{ph})}L_r}. \quad (8)$$

Thus

$$R_h = \frac{V_{R_f}}{\omega_{s(\text{ph})}L_r}. \quad (9)$$

Fig. 5 shows a circuit implementation of detecting $R_h = \gamma R_c$, in which the turns ratio $n = \omega_{s(\text{ph})}L_r/\gamma R_c$ and $\gamma > 1$. At the beginning, filament resistance $R_f = R_c$ and it can be shown that $V_{R_f} < \gamma R_c V_{L_r}/\omega_{s(\text{ph})}L_r$ so that the output of comparator CP_1 is close to ground level. Thus, Q_1 is in the off state and the switching frequency is determined only by R_T and C_1 . When R_f reaches $R_h = \gamma R_c$, the output of the comparator is pulled to V_{cc} , which turns on Q_1 and causes operating frequency changing from $\omega_{s(\text{ph})}$ to a frequency $\omega_{s(\text{fl})} (< \omega_{s(\text{ph})})$ at the full power rating. This frequency is determined by R_T and $C_1 + C_2$. When filament resistance reaches $R_h = \gamma R_c$, lamp is ready to be ignited. It usually takes 100–200 μs to go through an ignition process by changing the operating frequency. It is worth noting that with such a circuit for measuring I_{R_f} will not cost much because the magnetic core already exists for inductor L_r .

C. Determining dc-Link Voltage at Preheating Duration

During preheating interval, power imbalance may exist between the power factor correction semi-stage and the ballast semi-stage. Based on the law of energy conservation, the following equation can be derived:

$$\eta P_i \cdot \Delta t = P_d \cdot \Delta t + \frac{1}{2} C_c \cdot [(V_c + \Delta V)^2 - V_c^2] \quad (10)$$

where $\Delta V = V_c(t + \Delta t) - V_c(t)$, C_c is the dc-link capacitor, V_c is the dc-link voltage and η is the conversion efficiency of the buck-boost semi-stage, P_i denotes the input power, P_d denotes the dissipation power of the ballast semi-stage and Δt represents a small time interval. It can be shown that during filament-preheating interval, certain amount of input energy will accumulate in the dc-link capacitor. If input power P_i is not controlled from preheating transition through steady state operation, the voltage of dc-link capacitor at start-up transition will increase to a value much higher than that in steady state operation. For safety consideration, components with high voltage ratings must be used, increasing cost significantly. Therefore, the input power needs to be controlled at preheating stage.

In order to investigate dc-link voltage V_c varying with input power, it is necessary to analyze the lamp behavior at preheating transition. If the lamp does not generate glow current, it is treated as a resistor with infinite resistance during preheating interval, while the filaments are replaced with a resistor R_f . As a consequence, the ballast semi-stage is equivalent to a series-resonant series-loaded circuit, as shown in Fig. 4. The following equation can be derived from the proposed single-stage inverter and the circuit shown in Fig. 4

$$\begin{aligned} \eta \cdot \frac{V_I^2 d^2}{4L_{\text{pf}} f_{s(\text{ph})}} \cdot \Delta t \\ = 2 \cdot \frac{V_{Rf}^2}{R_f} \cdot \Delta t + \frac{1}{2} C_c \cdot [(V_c + \Delta V)^2 - V_c^2] \end{aligned} \quad (11)$$

where V_I is the amplitude of line voltage.

At the start-up transition, the power dissipated in the ballast semi-stage is divided into two parts: power loss in the inverter and the power dissipation in the filaments. Compared with the power dissipation of the filaments, the power loss in the inverter is not negligible. It is difficult to express the power dissipation in an equation analytically because R_f cannot be known explicitly. However, for convenience of discussion, a curve fitting technique is used to derive an expression for the power dissipation at the preheating interval. For instance, an expression of power dissipation P_d for a Philips T8 32W fluorescent lamp can be derived as follows:

$$P_d = \frac{\eta \cdot V_I^2 d^2}{4L_{\text{pf}} f_{s(\text{ph})}} \left(1 - e^{-(0.5d+8.6d^2)t}\right) \quad (12)$$

where $d = D(1 - e^{-t/RC})$ and D is the duty ratio at the steady state operation. This equation reveals that when t is large, P_d will approach to the power delivered by the PFC semi-stage. Thus, V_c will stop increasing. Combining (10), (11) and (12) can yield the following expression:

$$\begin{aligned} \eta \cdot \frac{V_I^2 d^2}{4L_{\text{pf}} f_{s(\text{ph})}} \cdot \Delta t = \frac{\eta \cdot V_I^2 d^2}{4L_{\text{pf}} f_{s(\text{ph})}} \left(1 - e^{-(0.5d+8.6d^2)t}\right) \\ \cdot \Delta t + \frac{1}{2} C_c \cdot [(V_c + \Delta V)^2 - V_c^2]. \end{aligned} \quad (13)$$

Thus, the dc-link voltage V_c at the end of preheating interval can be predicted from (13), and this result can assist engineers to choose components with proper ratings.

It can be observed from (13) that adjusting duty ratio can control dc-link voltage, which, in turn, controls component

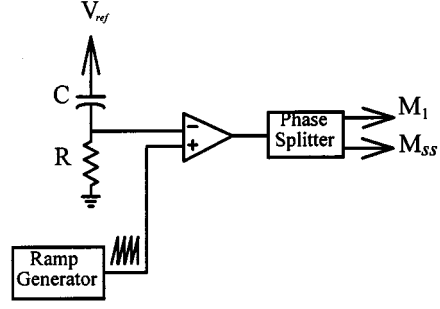
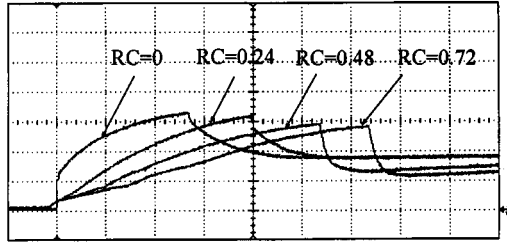


Fig. 6. Circuit for control duty ratio at start-up transition.

stresses. Many control circuits for reducing component stresses can be realized. A simple circuit, as shown in Fig. 6, is implemented in the following discussion. This circuit can control the duty ratio of gate driving signals for switches M_1 and M_{ss} to vary exponentially. Fig. 7 shows various measured waveforms of dc-link voltage corresponding to different RC time constants, lamp types and preheating frequencies. Fig. 7(a) shows the V_c waveforms for Philips T8 32W lamp operated at $f_{s(\text{ph})} = 79$ kHz and $f_{s(\text{fl})} = 47$ kHz. It can be observed that when $\gamma = R_h/R_c$ is fixed, a larger RC time constant will result in a lower V_c at ignition moment. Similarly, Fig. 7(b) shows the results for Philips T8 58W operated at $f_{s(\text{ph})} = 133$ kHz and $f_{s(\text{fl})} = 50$ kHz. Fig. 7(c) shows the V_c waveforms for T8 58W operated at $f_{s(\text{ph})} = 90$ kHz and $f_{s(\text{fl})} = 50$ kHz. From Fig. 7(b) and (c), it can be seen that when preheating frequency $f_{s(\text{ph})}$ is closer to full-load operating frequency, V_c can be further reduced. However, it has been observed from the experiment for obtaining the results shown in Fig. 7(c) that glow current through the lamp is not negligible during preheating stage, resulting in sputtering. Thus, a proper preheating frequency should be selected carefully so that glow discharge would not occur during preheating stage. Additionally, an optimal RC time constant should be selected while without delaying the start-up time and without losing chance in minimizing dc-link voltage V_c .

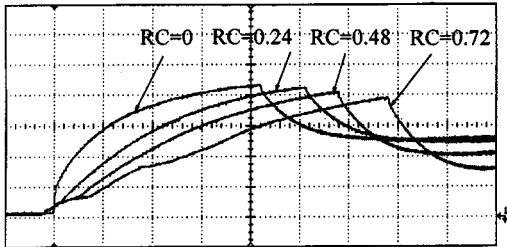
Fig. 8 shows the simulated results of V_c versus various RC time constants. Comparing Fig. 7(a) with Fig. 8 reveals that the obtained expression shown in (13) can predict dc-link voltage V_c precisely at the moment of ignition.

Combining both preheating ratio $\gamma = R_h/R_c$ detection circuit and duty ratio adjusting circuit can operate lamps more appropriately. Fig. 9 shows the measured V_c waveforms of a single-stage electronic ballast with the lamp of T8 58W, $f_{s(\text{ph})} = 133$ kHz, $f_{s(\text{fl})} = 50$ kHz, $RC = 0.48$ s and with various on-off time intervals. In the figure, Curve 1 represents a V_c trajectory when lamp starts from a cool filament resistance, and ignites at $\gamma = 4.2$. Curve 2 is the one when the lamp in the on-stage lasts for 1 minute and turns off for another 1 minute, and then turns on again. When the lamp in the on-stage lasts for 1 minute and turns off for 30 s, and then the lamp is ignited at $\gamma = 4.2$ again, another V_c trajectory (Curve 3) is measured and shown in the figure. Following the same procedure but reducing the off-time interval to 10 s, Curve 4 can be obtained. Among these four operating conditions, the on-state durations are kept constant. It can be seen from Fig. 9 that when the lamp lasts for



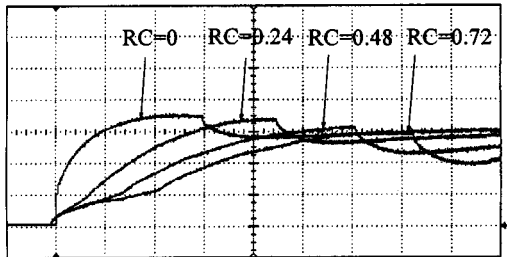
(100V/div, 200ms/div)

(a)



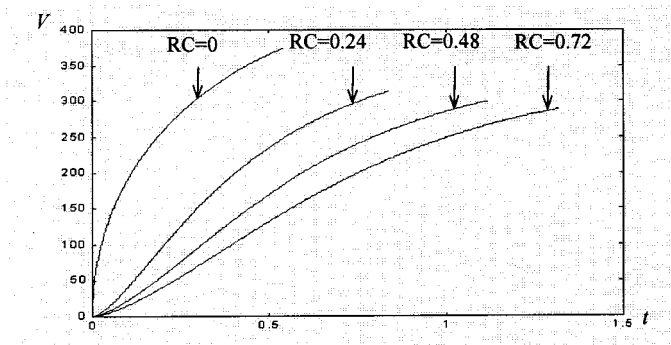
(100V/div, 200ms/div)

(b)

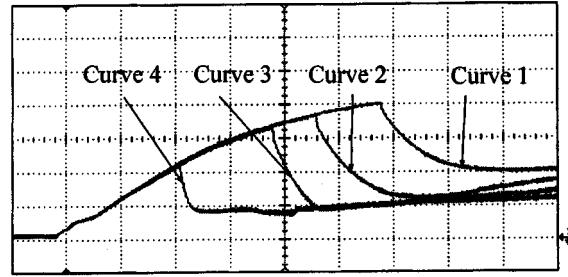


(100V/div, 200ms/div)

(c)

Fig. 7. Measured waveforms of dc-link voltage V_c .Fig. 8. Simulated waveforms of dc-link voltage V_c .

a shorter off-state interval and then re-ignites, filaments will reach a preheating ratio faster. This is because the filaments still



(100V/div, 200ms/div)

Fig. 9. Measured V_c waveforms versus various on-off operating intervals. Curve 1: starts with cool filaments, Curve 2: 1 min. on, 1 min. off, then ignites, Curve 3: 1 min. on, 30 s off, then ignites, and Curve 4: 1 min. on, 10 s off, then ignites.

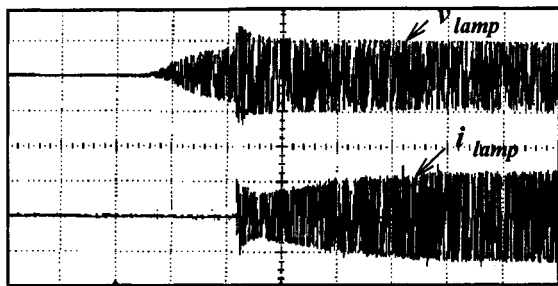
sustain a high temperature. With the γ detection circuit, lamps can be always ignited at a proper time moment regardless it is hot or cool. Thus, sputtering can be reduced effectively and so can the dc-link voltage be correspondingly reduced, resulting in improvements on component stresses.

IV. SIMULATED AND EXPERIMENTAL RESULTS

Another design example of the single-stage electronic ballast for a Philips T8 32W fluorescent lamp is presented to further verify the theoretical analysis. The ballast has been designed according to the following specifications.

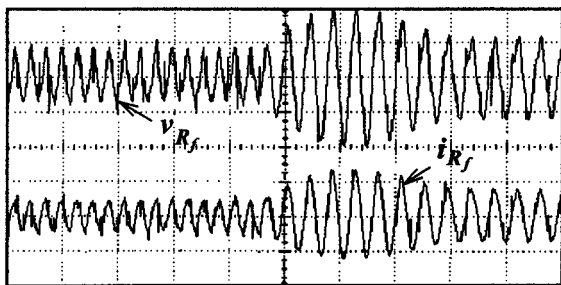
- 1) Input voltage: 120 V, 60 Hz.
- 2) Preheating frequency: 79 kHz.
- 3) Natural frequency: 50 kHz.
- 4) Switching frequency at the full load: 47 kHz.

Fig. 10 shows the lamp voltage and current waveforms during the preheating period, at which a significant voltage is generated across the lamp, while it does not induce undesired glow current. Fig. 11 shows the measured waveforms of the filament voltage and current around the igniting transition. The hot resistance ($R_h \approx 10.5 \Omega$) of the filament can be estimated from Fig. 11. Thus, the ratio of R_h to the cold resistance ($R_c = 2.5 \Omega$) can be determined as $R_h/R_c = 4.2$. The electrode reaches a temperature high enough for thermionic emission. Fig. 12 illustrates the lamp voltage and current at the time close to the glow-to-arc transition. From Fig. 12, it can be shown that the electrode was properly preheated by the relatively fast glow-to-arc transition. The measured results of dc-link voltage V_c shown in Fig. 7(a) illustrate that when the duty ratio is controlled by a simple RC circuit during the preheating interval, dc-link voltage V_c can be effectively reduced. Fig. 13 shows the input voltage and current waveforms, demonstrating a high input power factor and low current harmonics which are listed in Table I. These numbers meet the requirements of IEC 1000-3-2. Fig. 14 shows the simulated and measured waveforms of V_{DS} across MOSFET M_1 and I_{Lr} . These results reveal that a ZVS always exists at MOSFET M_1 turn-on transition because I_{Lr} starts with a negative current, which means the inverter operates above its resonance, at a switch turn-on transition (i.e., V_{DS} drops to zero).



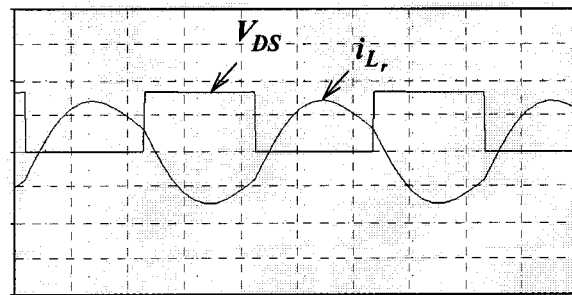
(200V/div, 0.2A/div, 500ms/div)

Fig. 10. Measured waveforms of the lamp voltage and current during the preheating period.



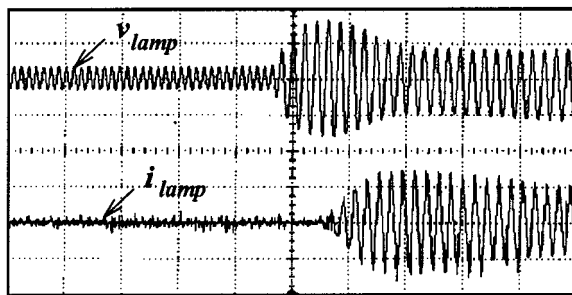
(20V/div, 2A/div, 50 μs/div)

Fig. 11. Measured waveforms of the filament voltage and current around the igniting transition.



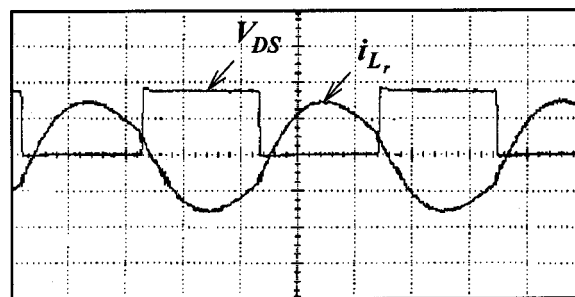
(100V/div, 0.4A/div, 5 μs/div)

(a)



(500V/div, 0.2A/div, 100 μs/div)

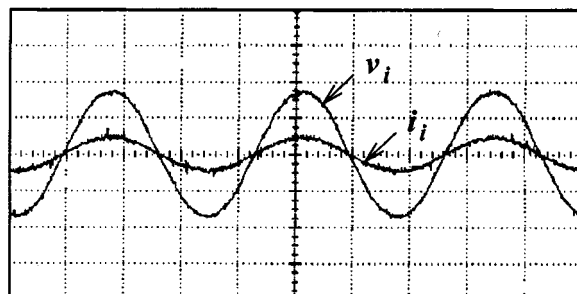
Fig. 12. Measured waveforms of the lamp voltage and current around the igniting transition.



(100V/div, 0.4A/div, 5 μs/div)

(b)

Fig. 14. (a) Simulated waveforms of V_{DS} across MOSFET M_1 , and I_{Lr} . (b) Measured waveforms of V_{DS} across MOSFET M_1 , and I_{Lr} .



(100V/div, 1A/div, 5ms/div)

Fig. 13. Measured waveforms of the input line voltage and current.

TABLE I
LIST OF THE POWER FACTOR
AND CURRENT HARMONICS

| | |
|---------------|-------|
| Power factor | 0.996 |
| THD | 3.78% |
| 3rd harmonic | 1.58% |
| 5th harmonic | 2.30% |
| 7th harmonic | 2.21% |
| 9th harmonic | 0.74% |
| 11th harmonic | 0.23% |
| 13th harmonic | 0.68% |
| 15th harmonic | 0.77% |

V. CONCLUSION

This paper presents the analysis and design of a high power factor single-stage electronic ballast considering start-up scenario. The proposed single-stage ballast is the combination of a buck-boost converter and a half-bridge series-resonant parallel-loaded inverter. Duty ratio is properly adjusted by a simple RC circuit in preheating duration; thus, dc-link voltage will not increase indefinitely and will not cause detrimental damage to the components. Switching devices with lower ratings can be used which, in turn, can effectively reduce the system cost and

increase the system reliability. In addition, a preheating ratio detection circuit has been proposed. Including this circuit can ensure that filaments always operate at a proper thermionic emission temperature, which results in reducing sputtering significantly.

A prototype of the ballast for a Philips T8 32W fluorescent lamp has been successfully implemented with practical consideration. Component stresses can be effectively reduced and long lamp life can be also effectively sustained without observing significant sputtering.

REFERENCES

- [1] R. Redl, L. Balogh, and N. O. Sokal, "A new family of single-stage isolated power-factor correctors with fast regulation," in *Proc. PESC'94*, 1994, pp. 1137–1145.
- [2] R. Redl and L. Balogh, "Design considerations for single-stage isolated power-factor-corrected power supplies with fast regulation of the output voltage," in *Proc. APEC'95*, 1995, pp. 454–459.
- [3] E. Deng and S. Cuk, "Single stage, high power factor, lamp ballast," in *Proc. APEC'94*, 1994, pp. 441–449.
- [4] C. Blanco, M. Alonso, E. Lopez, A. Calleja, and M. Rico, "A single stage fluorescent lamp ballast with high power factor," in *Proc. APEC'96*, 1996, pp. 616–621.
- [5] F. Okamoto and M. Mitani, "AC-DC-AC converter," U.S. Patent 2 133 940A, Jan. 13, 1984.
- [6] K. Senda, Inverter, Japan Patent 7-312 873, Nov. 28, 1995.
- [7] J. L. F. Vieira, M. A. C'o, and L. D. Zorzal, "High power factor electronic ballast based on a single power processing stage," in *Proc. PESC'95*, pp. 687–693.
- [8] I. Takahashi, "Power factor improvement of a diode rectifier circuit by dither signals," in *Proc. IAS'90*, 1990, pp. 1289–1294.
- [9] Y.-R. Yang and C.-L. Chen, "A self-excited half-bridge series-resonant ballast with automatic input current shaping," in *Proc. PESC'96*, 1996, pp. 881–886.
- [10] M. Maehara, "Inverter Setup," R.O.C. Patent 185 027, June 1, 1992.
- [11] W. Chen, F. C. Lee, and T. Yamauchi, "An improved "charge pump" electronic ballast with low THD and low crest factor," in *Proc. APEC'96*, 1996, pp. 622–627.
- [12] ———, "Reduction of voltage stress in charge pump electronic ballast," in *Proc. PESC'96*, 1996, pp. 887–893.
- [13] T.-F. Wu, M.-C. Ching, and E.-B. Chang, "Analysis and design of a high power factor, single-stage electronic ballast with dimming feature," in *Proc. IAS'97*, 1997, pp. 1030–1036.
- [14] E. Deng and S. Cuk, "Single switch, unity power factor, lamp ballasts," in *Proc. APEC'95*, 1995, pp. 670–344.
- [15] M. A. C'o, D. S. L. Simonetti, and J. L. F. Vieira, "High power factor electronic ballast operating at critical conduction mode," in *Proc. PESC'96*, 1996, pp. 962–968.
- [16] E. Statnic and G. Loehmann, "High power factor, high-frequency operating circuit for a low-pressure discharge lamp," U.S. Patent 5 521 467, May 28, 1996.

- [17] O. K. Nilssin, "Electronic Ballast with High Power Factor," U.S. Patent 4 985 664, Jan. 15, 1991.
- [18] C. S. Moo, Y. C. Chuang, and C. R. Lee, "A new power factor correction circuit for electronic ballasts with series-load resonant inverter," in *Proc. APEC'96*, 1996, pp. 628–633.
- [19] N. Nakagawa, "Inverter Setup," Japan Patent T-312 819, May 16, 1994.
- [20] R. O. Briochi, M. M. Lamego, and J. L. F. Vieira, "Constant Dc Link voltage HPF electronic ballast," in *Proc. IAS'97*, 1997, pp. 2353–2359.
- [21] T.-F. Wu and T.-H. Yu, "Off-line applications with single-stage converters," *IEEE Trans. Ind. Electron.*, vol. 44, pp. 638–647, Oct. 1997.
- [22] E. E. Hammer, "Photocell enhanced technique for measuring starting electrode temperatures of fluorescent lamps," in *Proc. IAS'97*, 1997, pp. 2313–2333.
- [23] E. E. Hammer and L. Nerone, "Performance characteristics of an integrally ballasted 20 W fluorescent quad lamp," *J. Illum. Eng. Soc.*, pp. 183–190, 1993.
- [24] W. R. Alling, "Important design parameters for solid-state ballasts," *IEEE Trans. Ind. Applicat.*, vol. 25, pp. 203–207, Mar./Apr. 1989.



Tsai-Fu Wu (S'89–M'91–SM'98) received the B.S. degree in electronics engineering from National Chiao-Tung University, Hsinchu, Taiwan, R.O.C., in 1983, the M.S. degree in electrical and computer engineering from Ohio University, Athens, in 1988, and the Ph.D. degree in electrical engineering and computer science from University of Illinois at Chicago (UIC) in 1992.

From 1985 to 1986 he was a System Engineer in SAMPO Inc., Taiwan, developing and designing graphic terminals. He was a Teaching and Research Assistant in the Department of Electrical Engineering and Computer Science, UIC, from 1988 to 1992. Since 1993, he has been with the Electrical Engineering Department, National Chung Cheng University, Chia-Yi, Taiwan, where he is a Professor and the Director of the Power Electronics Applied Research Laboratory (PEARL). His research interests include developing and modeling power converters, designing electronic dimming ballasts for fluorescent lamps and metal halide lamps, designing inverters for UPS applications, and designing solar-panel supplied inverters for grid connection.

Dr. Wu is a senior member of the CIE.



Yong-Jing Wu (S'98) was born in Kaohsiung, Taiwan, R.O.C., in 1971. He received the B.S. degree from Chung Yuan Christian University, Chung-Li, Taiwan, in 1996 and is currently pursuing the Ph.D. degree at National Chung Cheng University, Chia-Yi, Taiwan.

His research interests include developing and designing converter topologies, electronic ballasts, and high-efficient postregulators.